

OPTICAL STRUCTURE AND COLORS OF FAINT COMPACT NARROW EMISSION LINE GALAXIES¹

RAFAEL GUZMÁN,^{2,3,4} ANNA JANGREN,⁵ DAVID C. KOO,² MATTHEW A. BERSHADY,⁵ AND LUC SIMARD²

Received 1997 July 28; accepted 1997 December 23; published 1998 January 30

ABSTRACT

We present the results of *Hubble Space Telescope* Wide Field Planetary Camera imaging in V_{606} and I_{814} of five compact narrow emission line galaxies (CNELGs) and four slightly more extended faint blue galaxies (FBGs) with $20.3 \leq B \leq 22.4$ and redshifts $z \sim 0.22\text{--}0.66$. Half-light radii are measured to span from $0''.14$ to $0''.67$, thus yielding small sizes of $R_e \sim 1\text{--}5$ kpc ($H_0 = 50$ km s⁻¹ Mpc⁻¹, $q_0 = 0.1$). The new scale lengths, in combination with previous Keck measurements of velocity widths, continue to confirm that CNELGs, though quite luminous ($M_B \sim -21$), have masses comparable to dwarf galaxies (i.e., $M/M_\odot \lesssim 10^{10}$). Their low mass-to-light ratios are consistent with values corresponding to very early phases of a major burst of star formation. The spatial contour maps and surface brightness profiles of CNELGs reveal the presence of high surface brightness knots surrounded by a diffuse exponential-like component and sometimes accompanied by fans and tails. Since the knots tend to also have bluer colors, they are identified as the location of the current starburst. The diffuse component is interpreted to be an older underlying population. With the current burst estimated from the rest-frame ($B - V$) colors and mass-to-light ratios to involve typically $\sim 10\%$ of the galaxy mass, CNELGs are predicted to fade by ≤ 4 mag to reach the low luminosities and surface brightnesses of bright spheroidal galaxies, such as NGC 205. These new results provide further support for our previous suggestion that these distant, low-mass, starburst galaxies may be the progenitors of today's bright spheroidals. In contrast, although the four FBGs have similar colors and mass-to-light ratios to CNELGs, they will most likely not evolve into spheroidals but will resemble small, star-forming disk galaxies.

Subject headings: cosmology: observations — galaxies: compact — galaxies: evolution — galaxies: formation — galaxies: fundamental parameters

1. INTRODUCTION

Compact narrow emission line galaxies (CNELGs) are low-mass starburst systems at redshifts $z \lesssim 1$, similar to nearby H II galaxies (Koo et al. 1994, 1995; Guzmán et al. 1996; see also Phillips et al. 1997; Guzmán et al. 1997). Using single-burst evolutionary stellar population models, Koo et al. (1995) estimate that, without additional star formation, CNELGs can fade by $\Delta M_B \sim 4\text{--}7$ mag to match the low luminosities and surface brightnesses of spheroidal galaxies (Sphs; also called dwarf ellipticals). The assumption of no major star formation events after the current burst is consistent with energetic arguments that any remaining gas would be blown away in supernova-driven galactic winds (Dekel & Silk 1986; Guzmán et al. 1996). However, CNELGs may still have an underlying older population large enough to reduce the amount of fading and thus prevent them from reaching the low luminosities and surface brightnesses characteristic of Sphs. Such an underlying population has been observed in local blue compact dwarfs (Papaderos et al. 1996) and H II galaxies (Telles & Terlevich 1997). In this Letter, we reassess the amount of fading in CNELGs considering new evidence for an older, underlying stellar component revealed in the optical structure and colors of five CNELGs and four slightly more extended faint blue

galaxies (FBGs) observed with the Wide Field Planetary Camera (WFPC2) of the *Hubble Space Telescope* (HST). The observations and data reduction are described in § 2. The colors and optical structure are presented in § 3. The effect of the underlying population on the overall galaxy fading, and the implications for the connection between CNELGs and Sphs, are discussed in § 4. Throughout this Letter we adopt $H_0 = 50$ km s⁻¹ Mpc⁻¹ and $q_0 = 0.1$.

2. OBSERVATIONS AND DATA REDUCTION

The sample was chosen from a set of CNELGs and FBGs at $z \sim 0.03\text{--}0.7$ (Koo & Kron 1988). Ground-based measurements of magnitudes, colors, redshifts, and line strength ratios, as well as emission line velocity widths measured from high-resolution echelle spectra, are given in Koo et al. (1995). HST observations consist of two exposures taken with WFPC2 through filter V_{606} and another two exposures through I_{814} , with relative offsets of $\sim 1''$ from the first to second exposure in each filter. Total exposure times were 700 s in V_{606} (except for Herc 13925 and Herc 13088, which were observed for 800 s) and 900 s in I_{814} (except for Herc 13925 and Herc 13088, which were observed for 1000 s). The CNELGs were observed at the center of the Planetary Camera, while the FBGs were observed with the Wide Field Camera. The images were bias-subtracted, flat-fielded, cosmic-ray cleaned, and combined following standard procedures using IRAF tasks and our own software. Curves of growth were derived from circular aperture photometry centered at the intensity-weighted centroid in each filter (both before and after deconvolving with the PSF of the WFPC2) and used to measure the apparent total magnitudes and angular half-light radii (r_e). The effect of the PSF on these parameters is found to be negligible. We also measured various concentration indices that will be analyzed in a subsequent paper (Jangren et al. 1998). The photon noise error in the total

¹ Based on observations with the NASA/ESA *Hubble Space Telescope* (HST) obtained at the Space Telescope Science Institute (STScI), which is operated jointly by AURA, Inc., under NASA contract NAS5-26555.

² University of California Observatories/Lick Observatory, Board of Studies in Astronomy and Astrophysics, University of California, Santa Cruz, CA 95064; koo@ucolick.org, simard@ucolick.org.

³ Current address: Department of Astronomy, Yale University P. O. Box 208101, New Haven, CT 06520-8101; rguzman@astro.yale.edu.

⁴ Hubble Fellow.

⁵ Department of Astronomy and Astrophysics, Pennsylvania State University 525 Davey Lab, University Park, PA 16802; jangren@astro.psu.edu, mab@astro.psu.edu.

magnitudes is 0.01 mag. The r_e -values derived from the V_{606} and I_{814} images are very similar [i.e., $r_e(V_{606})/r_e(I_{814}) = 1.03 \pm 0.04$]. Since the redder image is more representative of any older, underlying population, we choose $r_e(I_{814})$ to parameterize the size of our sample galaxies. The typical uncertainty in these measurements is 7%. Curves of growth, total magnitudes, and sizes are used to derive apparent surface brightness profiles $\mu(r)$, absolute blue luminosities M_B , linear half-light radii R_e , and blue average surface brightnesses SB_e within R_e . We also measured $(V_{606} - I_{814})$ colors within an aperture whose diameter is approximately 4 times r_e . Finally, rest-frame $(B - V)$ aperture colors and gradients were derived using Fukugita et al.'s (1995) k -corrections and color transformations. The typical uncertainty in these values is estimated to be ~ 0.08 mag. This information is summarized in Figure 1 (Plates L1 and L2).

3. MORPHOLOGY, SURFACE BRIGHTNESS PROFILES, AND COLOR GRADIENTS

The contour maps of the V_{606} images for our galaxy sample are shown in the first column of panels in Figure 1. CNELGs show a variety of structure: compact cores surrounded by smooth, regular isophotes (SA 57–17731 or SA 57–5482); disturbed isophotes due to the presence of fans and tails (SA 57–7042); or multiple, smaller compact regions (SA 57–1501 or SA 57–10601). Similar morphologies have been observed in nearby H II galaxies (Telles & Terlevich 1997), suggesting the existence of large H II regions surrounded by an underlying population. To assess the relative importance of the current starburst in CNELGs as compared with any underlying component, we have isolated the compact regions (arguably, the location of the starburst). Following a similar procedure to that commonly used for nearby H II galaxies (e.g., Telles & Terlevich 1997), we first identify the underlying component by fitting an exponential law to the I_{814} surface brightness profile in the outer regions of the galaxy (i.e., outside R_e). The resulting disk scale length and central surface brightness are used to model a purely exponential object whose luminosity is scaled to the total galaxy luminosity in V_{606} . This model galaxy defines the diffuse underlying population, which is then subtracted from the original V_{606} galaxy image to produce the residual contour maps shown in the second column of panels in Figure 1. The residual maps reveal a major high surface brightness component in CNELGs that dominates the luminosity distribution within R_e . The size of such compact regions, as determined by their FWHM, is typically ~ 1 kpc. This size is characteristic of giant extragalactic H II regions such as 30 Dor in the Large Magellanic Cloud (Walborn 1991).

An alternative method for discriminating between the starburst and the underlying component is to construct a two-dimensional color map of the entire galaxy. Given the redshift range of most of our sample galaxies, the V_{606} and I_{814} filters map approximately into rest-frame B and V . A far more sensitive color for assessing possible stellar population differences within these extreme star-forming systems is, however, the rest-frame $(B - H)$ color (e.g., Salzer et al. 1998). Nevertheless, the smoothed $(V_{606} - I_{814})$ color maps do show that the compact regions shown in the residual maps correspond to the bluest regions in each galaxy [typically ~ 0.2 mag bluer than the surroundings in rest frame $(B - V)$], thus supporting our interpretation of the high surface brightness areas as the location of the most recent star formation.

The I_{814} surface brightness profiles $\mu(r)$ are shown in the third column of panels in Figure 1. Most CNELGs exhibit steep profiles, with the local surface brightness decreasing rapidly by ~ 5 mag at only $1''$ from the center. Superimposed on the data we show the fits to the outer regions adopted to model the underlying galaxy (*solid lines*). The profiles are often well fitted by an exponential law outside R_e , although they may also show small “bumps” due to the presence of fans, tails, and multiple compact regions revealed in the contour maps. Inside R_e , the profiles tend to show a significant enhancement in surface brightness corresponding to the compact bluer component described above. The overall galaxy profile can be well fitted using the generalized exponential function introduced by Sérsic (1968). The average power index derived for the CNELG sample is $n = 0.5_{-0.06}^{+0.10}$; i.e., the average profile is steeper than a simple exponential law ($n = 1.0$) but shallower than the typical profile of elliptical galaxies ($n = 0.25$). The exponential fits to the outer regions yield an average rest-frame blue central surface brightness $\mu_B^0 = 18.6 \pm 0.4$ mag arcsec $^{-2}$ for the CNELG sample. This value is about 3 mag brighter than that characteristic of spiral galaxies (Freeman 1970) but consistent with those observed in nearby H II galaxies (Telles & Terlevich 1997).

Finally, the rest-frame $(B - V)$ color gradients are shown in the fourth column. Within the uncertainties of our photometry, the observed gradients do not support significant color changes [i.e., $\Delta(B - V) > 0.2$ mag] across the galaxy in most CNELGs. There is, however, a slight trend in the gradients in the sense that the bluest color measurements are found normally in the inner regions of the galaxy. Indeed, the $(B - V)$ color of CNELGs within R_e is, on average, 0.14 ± 0.05 mag bluer than that outside R_e .

The remaining four FBGs differ from the CNELGs in the sense that FBGs exhibit larger angular and linear sizes; the bluer, higher surface brightness regions tend to be located outside the galaxy center and are more extended; the average central surface brightness derived from the exponential fits is about 1 mag fainter (i.e., $\mu_B^0 = 19.8 \pm 0.4$ mag arcsec $^{-2}$, closer to those values characteristic of small, high surface brightness disk galaxies; see Tully et al. 1998); and their color profiles tend to be bluer at larger radii (except for Herc 13088), more consistent with the observed color gradients in normal disk galaxies.

In summary, the structure, surface brightness profiles, and color gradients shown in Figure 1 suggest that CNELGs may be composed of two stellar components, as observed in other nearby low-mass starburst galaxies. Given the small number of objects in our sample, however, this preliminary result needs to be confirmed with larger data sets. In general, we distinguish a compact, bluer region within R_e that can be identified as the starburst region and a diffuse, generally redder and exponential-like component in the outer part. The presence of this underlying component suggests the existence of a stellar population formed previously to the current burst of star formation. The effect of such an older population on the luminosity evolution of CNELGs is discussed below.

4. THE CNELG-SPH EVOLUTIONARY SCENARIO REVISITED

In this section, we address whether CNELGs may evolve into today's Sph galaxies given the new evidence for an older underlying population. We include in this analysis seven other CNELGs whose structural and kinematical properties are pub-

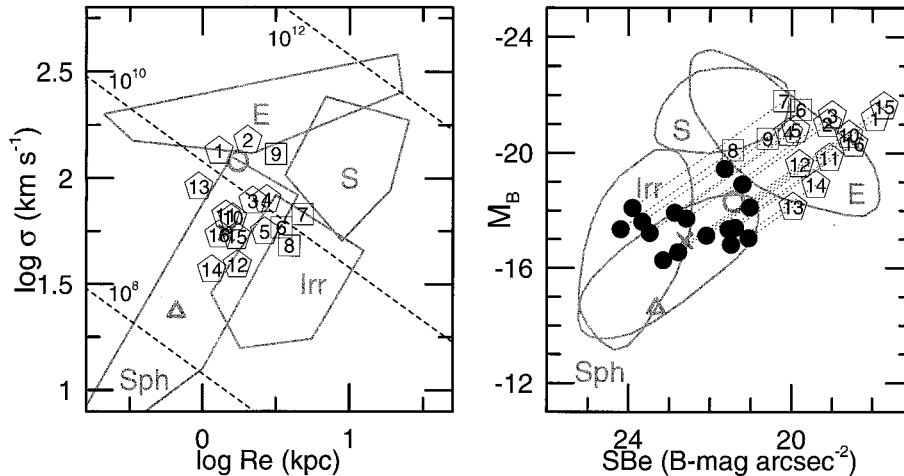


FIG. 2.—(a) $\log R_e$ in kpc vs. $\log \sigma$ in km s⁻¹ for 12 CNELGs (pentagons) and four FBGs (squares). Velocity widths were increased by $\sim 30\%$ to account for the systematic difference between velocity widths and true circular velocities (Guzmán et al. 1996; Rix et al. 1997). Identification numbers are listed in Table 1. Dashed lines represent constant mass of 10^8 , 10^{10} , and $10^{12} M_\odot$, respectively. Solid lines represent the typical location of elliptical (E), spiral (S), irregular (Irr), and spheroidal (Sph) galaxies. Symbols with no labels represent the values of three typical spheroidal galaxies (triangle, NGC 147; cross, IC 3393; circle, NGC 3605). (b) SB_e vs. M_B . Point symbols as before. Dotted lines show the predicted luminosity evolution for each galaxy from its lookback time until the present. Filled circles represent the final faded positions.

lished in Koo et al. (1994) and Guzmán et al. (1996). The combined data set nearly doubles our previous sample.

In Figures 2a and 2b, we show the R_e - σ and M_B - SB_e diagrams for the combined sample as well as the schematic locus of various nearby galaxy types (see Guzmán et al. 1996; Phillips et al. 1997; and references therein). These two diagrams provide useful descriptions of the global structural properties of galaxies. As previously reported, the high blue luminosities and surface brightnesses of CNELGs, together with their small sizes and velocity widths, are consistent with their being low-mass ($M \lesssim 10^{10} M_\odot$), extreme star-forming systems similar to nearby H II galaxies (Koo et al. 1994, 1995; Guzmán et al. 1996). Since R_e and σ are roughly independent of the fading of the stellar population, the R_e - σ diagram allows a direct comparison between the properties of these distant, low-mass starbursts and those of nearby, quiescent stellar systems. The vast majority of CNELGs lie on top of the observed distribution of nearby Sph galaxies (SA 57-17731 and SA 57-7042 are in the transition zone between bright Sph and intermediate E galaxies). Although the position of CNELGs in this diagram may vary slightly as they evolve, we have argued that there is no evidence against CNELGs being related structurally and kinematically to today's bright spheroidals (Guzmán et al. 1996). The FBGs, however, deviate from the Sph sequence, with Herc 13088, SA 57-4259, and SA 57-3605 having R_e - and σ -values more similar to those of irregular galaxies, and Herc 13925 being most likely a small spiral galaxy, as inferred from its disklike morphology and exponential light profile.

A key issue for the evolutionary link between CNELGs and Sphs is whether the former will fade enough to reach the low luminosities and surface brightness characteristic of the latter. Koo et al. (1995) concluded that, without previous or subsequent star formation, CNELGs can fade by $\Delta M_B \sim 4-7$ mag. Given the evidence for two stellar components in CNELGs, we reestimate the amount of fading using two-burst evolutionary population models of Sph galaxies (Schmidt, Alloin, & Bica 1995). We assume that CNELGs are undergoing their last major burst of star formation, since galactic winds following the current burst are likely to remove most of the remaining

gas (Guzmán et al. 1996). The models describe the evolution of the blue luminosity, optical colors, and line strengths of a typical Sph (i.e., $M_B \sim -17$, $Z = 0.3 Z_\odot$, and $B - V = 0.9$) that has experienced a second instantaneous burst of star formation 3 Gyr ago involving 1% and 10% of the total galaxy mass. We also use Leitherer & Heckman's (1995) model predictions for the evolution of M_B and $(B - V)$ over the first 10^9 yr after a single, instantaneous burst with $Z = 0.25 Z_\odot$, and Worthey's (1994) model predictions for a similar single burst over the next 1-12 Gyr. Figure 3 shows the evolution of the

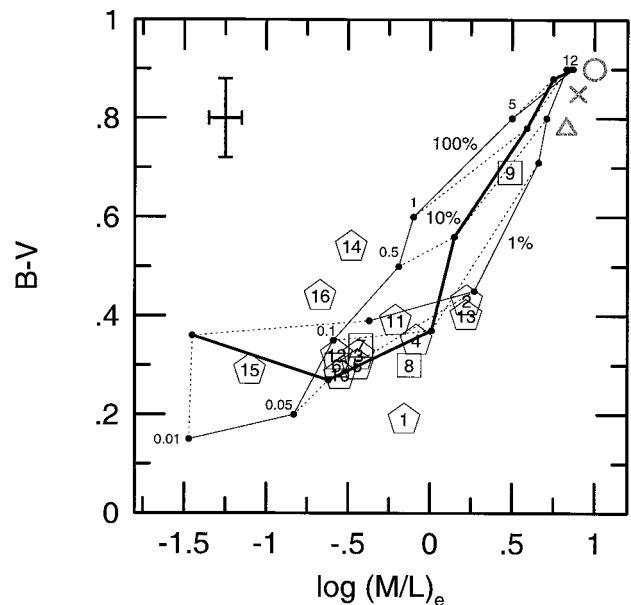


FIG. 3.— $\log (M/L)_e$ vs. $(B - V)$ for the combined data set. Point symbols as in Figure 2. Solid lines represent the model predictions for the evolution of a typical Sph galaxy after a single initial burst of star formation, and after a second burst involving 1% and 10% (thick solid line) of the total galaxy mass. Dots in the model lines correspond to ages 0.01, 0.05, 0.1, 0.5, 1, 5, and 12 Gyr. The error bar represents the typical uncertainty in our measurements.

TABLE 1
THE PREDICTED FADING FOR EACH GALAXY FROM ITS LOOKBACK TIME
UNTIL THE PRESENT

ID	z	t (Gyr)	$(B - V)^a$	$\log(M/L_B)_e^b$	ΔM_B	Number
SA 57-17731	0.663	7.3	0.19	-0.156	2.57	1
SA 57-7042	0.525	6.4	0.43	0.224	1.62	2
SA 57-5482	0.453	5.8	0.32	-0.435	3.26	3
SA 57-1501	0.499	6.2	0.35	-0.084	2.38	4
SA 57-10601	0.438	5.7	0.30	-0.443	3.28	5
Herc -13088	0.436	5.7	0.30	-0.569	3.60	6
SA 57-4259	0.601	7.0	0.34	-0.421	3.23	7
SA 57-3605	0.392	5.3	0.30	-0.126	2.49	8
Herc -13925	0.220	3.2	0.69	0.488	0.95	9
LYNX 2-11378	0.269	3.8	0.28	-0.550	3.55	10
LYNX 2-8115	0.197	3.1	0.39	-0.210	2.70	11
LYNX 2-11500	0.193	3.0	0.32	-0.570	3.60	12
Herc -13385	0.095	1.6	0.40	0.220	1.62	13
Herc -3618	0.132	2.4	0.54	-0.480	3.38	14
SA 68-17255	0.348	4.8	0.29	-1.100	4.93	15
SA 68-6134	0.285	4.2	0.44	-0.670	3.85	16

^a Rest-frame colors for objects 10–16 were derived from UJFN photometry.

^b Mass-to-light ratios are in solar units. Velocity widths used to calculate virial masses were increased by $\sim 30\%$ to represent the true circular velocities (Guzmán et al. 1996; Rix et al. 1997).

galaxy mass-to-light ratio $(M/L_B)_e$ within R_e and $(B - V)$ color predicted by the 1%, 10%, and single-burst models. In all cases, the variation in $(M/L_B)_e$ was derived from the change in blue luminosity predicted by the various models, assuming that the total galaxy mass remains constant and is normalized to $(M/L_B)_e = 7.5M/L_{B\odot}$. This value is representative of Sphs over a ~ 4 mag range in blue luminosity. Superimposed on the models, we show the combined data set of 12 CNELGs (*pentagons*) and four FBGs (*squares*). Galaxy $(M/L_B)_e$ ratios were estimated via the virial theorem as described in Guzmán et al. (1996). Given the typical uncertainty in our measurements and the overlap between the various evolutionary tracks, it is not possible to identify unambiguously the age and strength of the current burst for each galaxy.

However, the observed distribution of CNELGs in the $(M/L_B)_e$ - $(B - V)$ diagram is statistically consistent with their being Sph galaxies undergoing a second burst of star formation that involved $\sim 10\%$ of the galaxy mass. Under this assumption, the age of the second burst in CNELGs is estimated to be in the range ~ 0.01 to ~ 0.1 Gyr. The 10% second-burst model is thus used to predict the amount of fading for all objects but Herc 3618 and SA 68-6134, whose positions in the $(M/L_B)_e$ - $(B - V)$ diagram are more consistent with the single-burst model predictions. The predicted fading for each galaxy from its lookback time (t) until the present is listed in Table 1 and is typically less than ~ 4 mag. This is 2–3 mag less than our previous estimate based on single-burst models. The fading does not depend greatly on the adopted value for H_0 . On average, these estimates differ from those derived using $H_0 = 70 \text{ km s}^{-1} \text{ Mpc}^{-1}$ by less than ~ 0.2 mag.

Figure 2b shows the predicted positions of the 12 CNELGs in the M_B - SB_e diagram after fading. Indeed, CNELGs do have faded blue luminosities and surface brightnesses, as well as sizes and velocity widths, totally consistent with those of nearby bright Sph galaxies. Further support for the close evolutionary relation of CNELGs with Sph galaxies is provided by the intrinsic shapes of these galaxies. For instance, the average values of the faded blue luminosity and the power index n of the surface brightness profiles in CNELGs agree remarkably well with the observed distribution of bright Sph galaxies in the

M_B - n diagram (see Jerjen & Binggeli 1997). A similar conclusion has been drawn from the comparison of the intrinsic shapes of nearby blue compact dwarfs and Sph galaxies (Sung et al. 1997). Alternatively, the faded positions of FBGs clearly deviate from the sequence that Sph galaxies define in the M_B - SB_e diagram. In agreement with the discussion above on the R_e - σ diagram, the faded luminosities and surface brightnesses of SA 57-4259, SA 57-3605, and Herc 13088 are more consistent with those values of irregulars. These faded values were derived under the assumption that there was no further episode of star formation after the current burst. Since irregular galaxies are currently forming stars, the amount of fading for these three galaxies was overestimated from our models. The “true” position of these objects after fading is more likely to be closer to that of the brightest irregulars (i.e., $M_B \sim -19$, $SB_e \sim 23 \text{ mag arcsec}^{-2}$). A similar argument applies to Herc 13925, which is likely to fade only ~ 1 mag to become a low-luminosity (i.e., $M_B \sim -20$, $SB_e \sim 21.5 \text{ mag arcsec}^{-2}$) spiral galaxy. These results thus suggest that the majority of FBGs, typically more extended than CNELGs, are *not* related to today’s Sph galaxies.

In conclusion, the new, larger data set analyzed here supports our previous claim that CNELGs are low-mass starburst galaxies that are likely to evolve into the present population of bright Sph galaxies. Our analysis includes the effect of an older underlying component on the total fading of the stellar population after the current burst evolves, assuming this burst involves $\sim 10\%$ of the galaxy mass. This assumption is justified by the $(B - V)$ colors and $(M/L)_e$ ratios of CNELGs as compared with two-burst galaxy evolution models. However, it would be possible to quantify directly the strength of the current burst from the rest-frame $(B - H)$ color maps of CNELGs. These color maps have also proven key to determining unambiguously the extent and characteristics of the underlying population in nearby blue compact dwarfs (Salzer et al. 1998). NICMOS imaging of CNELGs would be most useful for investigating the properties of the underlying population of these distant low-mass starbursts and their relation to similar galaxies today.

Funding for this work was provided by NSF grant AST95-29098, NASA grant GO-05994.01-94A, and AR-07519.01

(A. J. and M. A. B.). R. G. also acknowledges partial support from the Hubble Fellowship grant HF-01092.01-97A.

REFERENCES

- Dekel, A., & Silk, J. 1986, *ApJ*, 303, 39
Freeman, K. C. 1970, *ApJ*, 160, 811
Fukugita, M., Shimasaku, K., & Ichikawa, T. 1995, *PASP*, 107, 945
Guzmán, R., Gallego, J., Koo, D. C., Phillips, A. C., Lowenthal, J. D., Faber, S. M., Illingworth, G. D., & Vogt, N. P. 1997, *ApJ*, 489, 559
Guzmán, R., Koo, D. C., Faber, S. M., Illingworth, G. D., Takamiya, M., Kron, R. G., & Bershad, M. A. 1996, *ApJ*, 460, L5
Jangren, A., et al. 1998, in preparation
Jerjen, H., & Binggeli, B. 1997, preprint (astro-ph/9701221)
Koo, D. C., Bershad, M. A., Wirth, G. D., Stanford, S. A., & Majewski, S. R. 1994, *ApJ*, 427, L9
Koo, D. C., Guzmán, R., Faber, S. M., Illingworth, G. D., Bershad, M. A., Kron, R. G., & Takamiya, M. 1995, *ApJ*, 440, L49
Koo, D. C., & Kron, R. G. 1988, *ApJ*, 325, 92
Leitherer, C., & Heckman, T. M. 1995, *ApJS*, 96, 9
Papaderos, P., Loose, H. H., Thuan, T. X., & Fricke, K. J. 1996, *A&AS*, 120, 207
Phillips, A. C., Guzmán, R., Gallego, J., Koo, D. C., Lowenthal, J. D., Vogt, N. P., Faber, S. M., & Illingworth, G. D. 1997, *ApJ*, 489, 543
Rix, H.-W., Guhathakurta, P., Colless, M., & Ing, K. 1997, *MNRAS*, 285, 779
Salzer, J. J., Elston, R., Sudarsky, D., & Sinnott, C. 1998, in preparation
Sérsic, J. L. 1968, *Atlas de Galaxias Australes* (Córdoba: Obs. Astron.)
Schmidt, A. A., Alloin, D., & Bica, E. 1995, *MNRAS*, 273, 945
Sung, E. C., Han, C., Ryden, B., Chun, M. S., & Kim, H. I. 1997, preprint (astro-ph/9709176)
Telles, E., & Terlevich, R. 1997, *MNRAS*, 286, 183
Tully, R. B., Verheijen, M. A. W., Pierce, M. J., Huang, J. S., & Wainscoat, R. J. 1998, *AJ*, in press
Walborn, N. R. 1991, in *Massive Stars in Starbursts*, ed. C. Leitherer, N. R. Walborn, T. M. Heckman, & C. A. Norman (Cambridge: Cambridge Univ. Press), 145
Worthey, G. 1994, *ApJS*, 95, 107

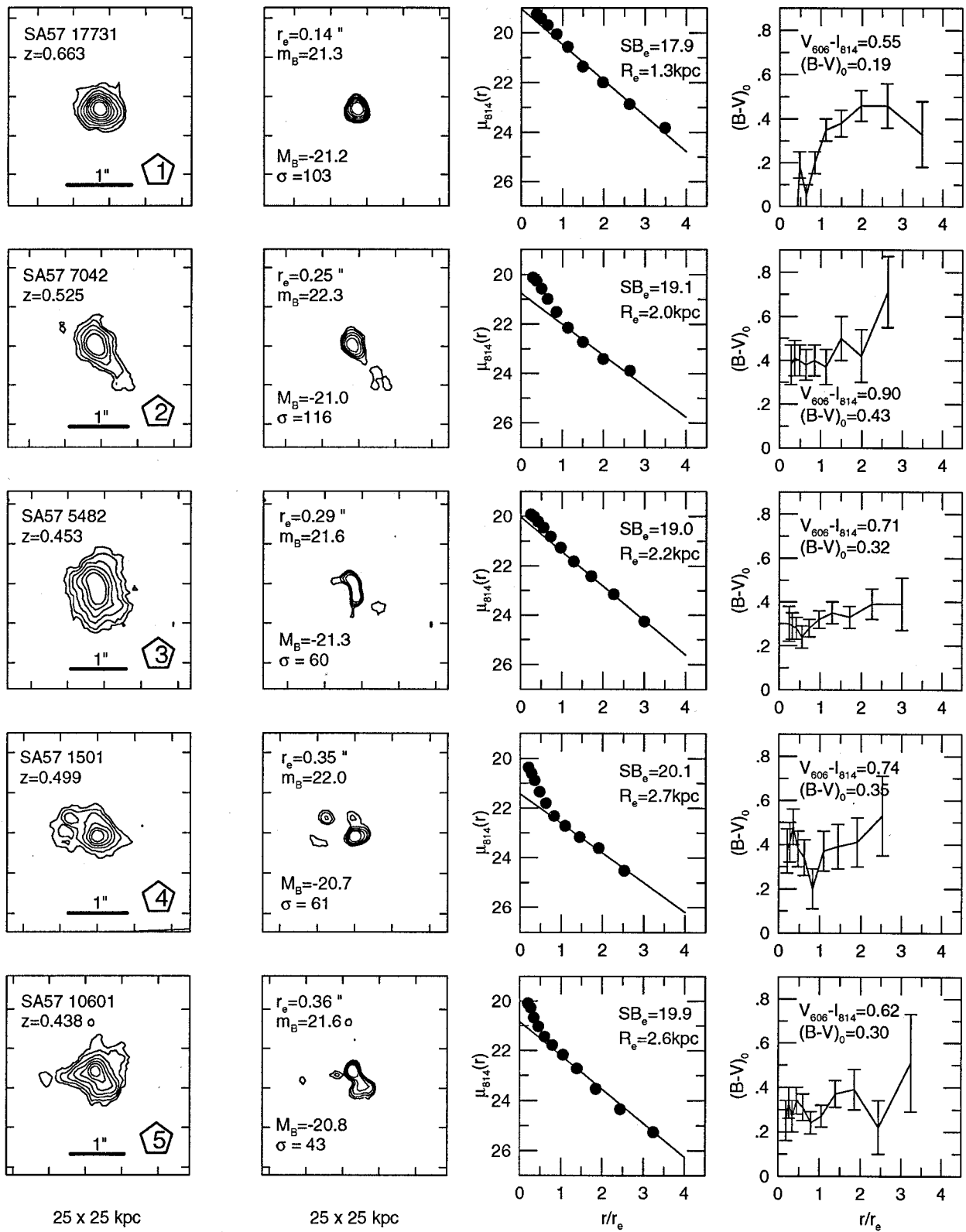


FIG. 1.—This figure shows four panels for each galaxy. The object identification is encoded in a symbol at the bottom right corner of the first panel (*pentagons*, CNELGs; *squares*, FBGs). The first panel is the V_{606} galaxy contour map in 0.5 mag intervals. The outermost contours correspond to 0.5 mag above sky level (i.e., $V_{606} \sim 23$ mag arcsec $^{-2}$). The contours are slightly smoothed, typically block-averaged by 3×3 pixels. The size of the panel is 25×25 kpc, while the horizontal scale represents $1''$. The second panel shows the residual contour maps of the high surface brightness component after the underlying, exponential-like component has been removed (see text). The third panel shows the I_{814} surface brightness profiles $\mu(r)$. The size of the data points is representative of the typical uncertainty in our measurements. The fourth panel shows the rest-frame $(B - V)_0$ color gradient.

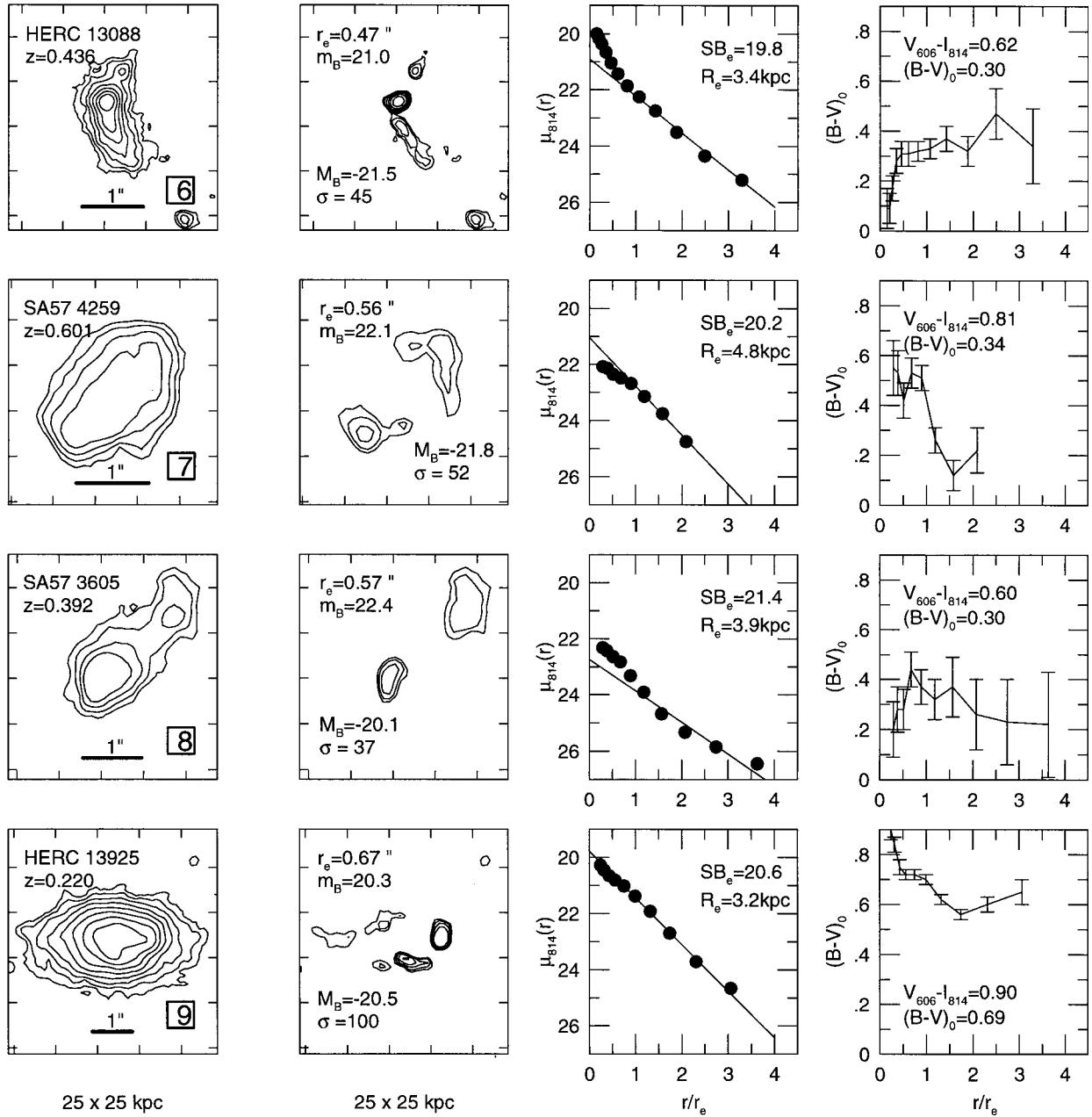


FIG. 1—Continued

GUZMÁN et al. (see 495, L14)